ACS Chemical Neuroscience

pubs.acs.org/chemneuro Research Article

Design, Synthesis, and Activity Study of Cinnamic Acid Derivatives as Potent Antineuroinflammatory Agents

Shun Huang, Wenfeng Liu,* Yonglian Li, Kun Zhang, Xi Zheng, Hubing Wu, and Ganghua Tang

Cite This: *ACS Chem. Neurosci.* 2021, 12, 419–429 Read Online

ACCESS | Metrics & More | Article Recommendations | Supporting Information

ABSTRACT: Neuroinflammatory cytokines are promising therapeutic targets for the treatment of Alzheimer's disease. Herein, we described our efforts toward the investigation of cinnamic acid derivatives as antineuroinflammatory agents. Intensive structural modifications led to the identification of compound **4f** as the most effective antineuroinflammatory agent *in vitro*. The oral administration of compound **4f** could reverse lipopolysaccharide (LPS)-induced memory disturbance and normalize glucose uptake and metabolism in the brains of mice. Further biological studies *in vivo* revealed that compound **4f** was directly bound to the mitogen-activated protein kinase (MAPK) signaling pathway, resulting in suppression of its downstream signaling pathway by blocking neuroinflammatory progression. Docking studies showed that compound **4f** could be inserted into the active pocket of interleukin-1β (IL-1β). Furthermore, it was confirmed that compound **4f** formed hydrogen bonds with SER84 to enhance the binding affinity. Taken together, these results are of great importance in the development of cinnamic acid derivatives for the treatment of Alzheimer's disease.

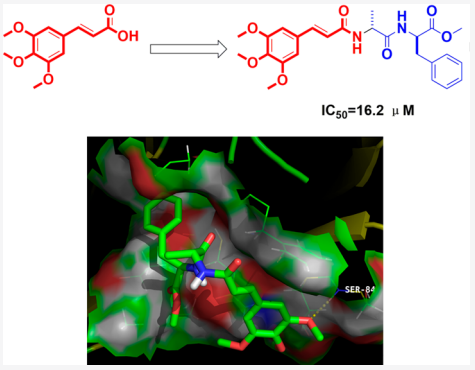

KEYWORDS: *Cinnamic acid derivatives, lipopolysaccharide, neuroinflammation, Alzheimer's disease*

INTRODUCTION

Alzheimer's disease (AD), a devastating neurodegenerative disease, is characterized by age-related memory loss and progressive cognitive impairment.[1] Accumulating evidence has shown that neuroinflammation is one of the neuropathological hallmarks of AD.[2,3] Once stimulated, signal-dependent transcription factors, including mitogen-activated protein kinase (MAPK) and nuclear factor-κB (NF-κB), are activated in neuroinflammatory processes to up-regulate the expression of downstream proinflammatory cytokines, such as interleukin-1β (IL-1β), IL-6, and tumor necrosis factor-α (TNF-α).[4] Moreover, microglia-dominated neuroinflammation, in response to various stimuli, has been shown to promote the overexpression of various neuroinflammatory cytokines, leading to astrocyte activation and neuronal damage.[5−7] Under neuroinflammatory conditions, neuronal damage can facilitate microglial and astrocyte activation, which, in turn, produces a cycle of constant neuroinflammation.[8−12] Importantly, sustained and chronic neuroinflammatory processes and progressive neuronal damage expedite the injury of brain tissue, which ultimately results in the development of behavioral pathology.[13] This suggests that the inhibition of neuroinflammation is a potentially viable strategy for the treatment of AD. However, few therapeutic agents modifying neuroinflammation have been reported to relieve the symptoms of AD. Therefore, new anti-AD agents are demanded.

Cinnamic acid, a major constituent of cinnamon (*Cinnamomum cassia*), is responsible for the pharmacological properties of cinnamon, which include anti-inflammatory, antimicrobial, antigastric, and antitumor activities.[14−17] Cinnamic acid is widely used as a plant-derived spice and flavoring agent in nutritional supplements. Cinnamic acid derivatives were confirmed to exert significant neuroprotective and anti-inflammatory effects by reducing Aβ-induced reactive oxygen species (ROS) and proinflammatory cytokines.[18,19] Accumulating evidence has identified cinnamic acid and its derivatives as potent antineuroinflammatory agents that could be repositioned as therapeutic candidates to treat many neurodegenerative diseases, notably in AD.[20,21] D-amino acids, which have been used in the preparation of sweeteners and as food and nutritional supplements,[22,23] and their peptides have received increasing attention in the treatment of inflammatory diseases.[24−26]

A recent study reported that modifying the structural skeletons of active constituents from natural products was an effective way to find lead compounds.[27] To date, numerous

Received: September 3, 2020
Accepted: January 7, 2021
Published: January 13, 2021

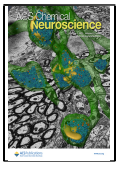

https://dx.doi.org/10.1021/acschemneuro.0c00578
ACS Chem. Neurosci. 2021, 12, 419–429

Scheme 1. Synthesis of the Target Compounds[a]

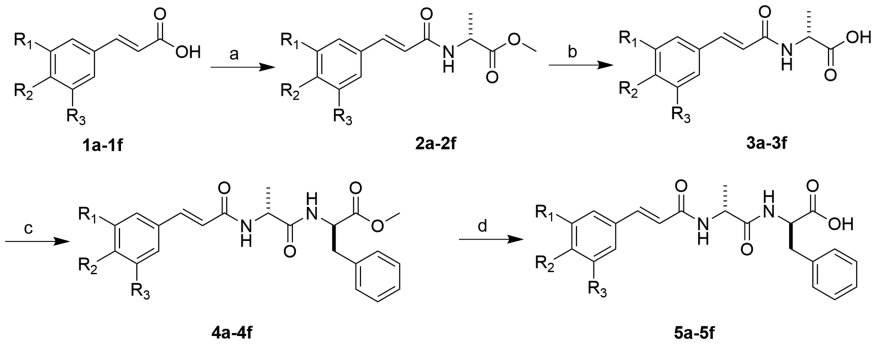

[a]Reagents and conditions: (a) methyl D-alaninate hydrochloride, EDC·HCl, HOAt, TEA, and DCM, at room temperature (rt) for 4 h; (b) LiOH and MeOH-THF-H_2O, at rt for 2 h, and then HCl; (c) methyl D-phenylalaninate hydrochloride, EDC·HCl, HOAt, TEA, and DCM, at rt for 4 h; (d) LiOH and MeOH-THF-H_2O, at rt for 2 h, and then HCl.

effective agents, natural compounds conjugated to other active constituents, have been widely used to treat AD.[28,29] Inspired by those results, we proposed to design and synthesize 24 cinnamic acid derivatives containing D-amino acid or peptides, with the aim of identifying unique antineuroinflammatory agents against AD. Furthermore, the antineuroinflammatory capacity of the cinnamic acid derivatives was assessed by their ability to inhibit the production of nitric oxide (NO) and IL-1β in an *in vitro* system and an *in vivo* model, and the antineuroinflammatory mechanisms of compound **4f** were investigated to reveal new insight into its therapeutic potential for AD.

RESULTS AND DISCUSSION

The synthetic route used for the preparation of cinnamic acid derivatives is shown in Scheme 1. Briefly, the synthesis of compounds **2a−f** began with the amidation of substituted cinnamic acids (**1a−f**) with methyl D-alaninate hydrochloride and was followed by a hydrolytic reaction with lithium hydroxide to yield intermediate **3a−f** (Scheme 1). Then compounds **3a−f** were mixed with commercially available methyl D-phenylalaninate hydrochloride to afford compounds **4a−f** through an amidation reaction in the presence of triethylamine. Similarly, compounds **4a−f** were hydrolyzed with lithium hydroxide to afford compounds **5a−f**. Finally, 24 compounds were synthesized in the present study. The yields ranged from 54.1 to 89.3%, and the purity of the target compounds was >92%.

It has been demonstrated that cinnamic acid and its derivatives can be effective therapeutical agents for the treatment of AD by inhibiting neuroinflammatory activity.[18−20] Herein, we investigated their inhibitory effect on NO production *in vitro*. As shown in Table 1, resveratrol (Res) at an initial concentration of 20 μM showed 77.01% inhibition against NO production. Thus, we used Res as the positive control and investigated the inhibitory effect of 24 compounds at 20 μM on NO production. Compared to that of Res, most of the synthesized compounds exhibited potent inhibitory activity against NO production. Among them, compound **4f** at 20 μM displayed potent inhibitory activity (62.72%) compared to that of the other compounds, with an IC_{50} value of 16.2 μM. Compound **4d** showed moderate activity at 42.57% inhibition (Table 1). Structure−activity relationship (SAR) studies showed the activity of the target compounds against NO production in lipopolysaccharide (LPS)-induced BV2 microglia cells in the descending order of **4f** > **4d** > **3d** > **4a** > 30%. Compounds **4a**, **4d**, and **4f**, with substituents at the R_4 position (R_4 = CH_3), exhibited significantly higher inhibition rates of 31.09, 42.57, and 62.72%, respectively, at 20 μM. Compound **4f** with −OCH_3 at the R_1, R_2, and R_3 positions was the most potent compound against LPS-induced NO production.

Table 1. Effect of the Compounds on NO Production

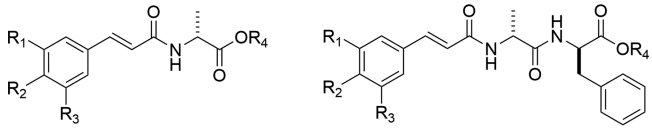

2a-2f and 3a-3f 4a-4f and 5a-5f

ID	R_1	R_2	R_3	R_4	inhibition at 20 μM (%)	NO IC_{50} (μM)[a]
2a	H	H	H	CH_3	10.69	>20
2b			CH_3		25.06	>20
2c			OCH_3		21.73	>20
2d			F		14.52	>20
2e			CF_3		17.51	>20
2f	OCH_3	OCH_3	OCH_3		29.46	>20
3a	H	H	H	H	14.39	>20
3b			CH_3		24.83	>20
3c			OCH_3		24.94	>20
3d			F		31.26	>20
3e			CF_3		9.90	>20
3f	OCH_3	OCH_3	OCH_3		29.35	>20
4a	H	H	H	CH_3	31.09	>20
4b			CH_3		11.08	>20
4c			OCH_3		20.62	>20
4d			F		42.57	>20
4e			CF_3		20.09	>20
4f	OCH_3	OCH_3	OCH_3		62.72	16.2
5a	H	H	H	H	16.19	>20
5b			CH_3		12.41	>20
5c			OCH_3		13.75	>20
5d			F		26.61	>20
5e			CF_3		14.06	>20
5f	OCH_3	OCH_3	OCH_3		11.83	>20
Res					77.01	11.9

[a]Concentration (μM) for 50% inhibition of NO release in BV2 cells. The IC_{50} values are the mean ± SD of at least three experimental determinations.

https://dx.doi.org/10.1021/acschemneuro.0c00578
ACS Chem. Neurosci. 2021, 12, 419−429

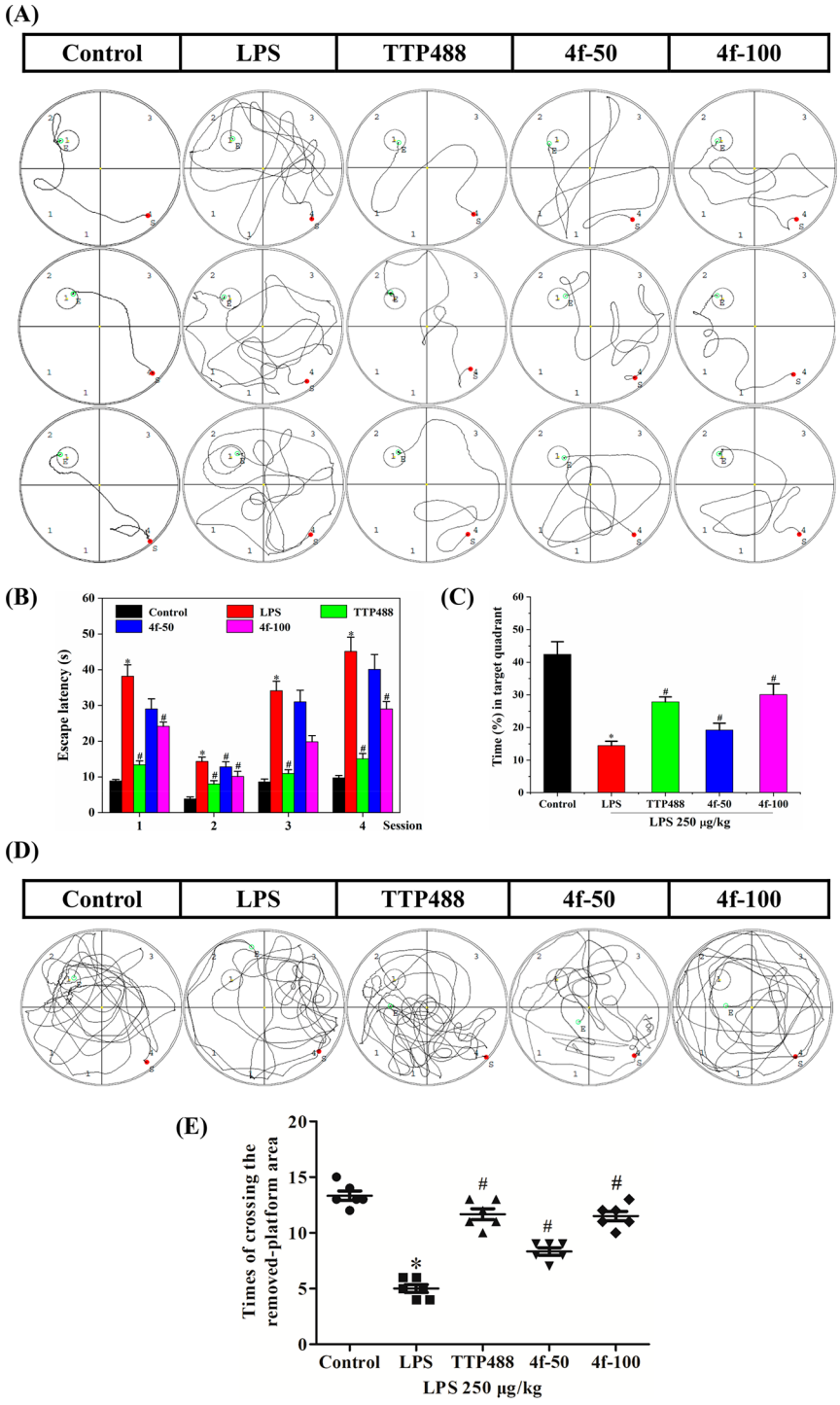

Figure 1. Effects of compound **4f** on LPS-induced memory impairment. (A) Movement tracks of mice in the place navigation (hidden-platform) test. (B) The escape latency time of mice in the place navigation (hidden-platform) test. (C) The percentage of time the mice spent searching for the target quadrant in the spatial probe test. (D) Movement tracks of the mice in the spatial probe test. (E) The number of times the mice crossed the removed-platform area in the spatial probe test. The significance of differences from control group at $*p < 0.05$, from LPS group at $\#p < 0.05$.

Accordingly, compound **4f** was selected for further investigation of the antineuroinflammatory mechanism of action.

The systemic administration of LPS has been reported to cause memory impairment and learning disabilities.[30] Herein, we performed the Morris water test (MWM) test to determine the effects of compound **4f** on LPS-induced memory impairment and learning disability. As shown in Figure 1A,B, LPS treatment caused a cognitive deficiency ($p < 0.05$) and an increase in the escape latency time compared to that of the control group, whereas the oral administration of compound **4f** dose-dependently decreased the escape latency time in the second session ($p < 0.05$). In addition, the escape latency time of the TTP488 group was lower than that of the LPS group mice in the first, second, third, and fourth sessions. Moreover, the results demonstrated that the movement tracks of the mice were consistent with the escape latencies in 2 min. The

https://dx.doi.org/10.1021/acschemneuro.0c00578
ACS Chem. Neurosci. 2021, 12, 419−429

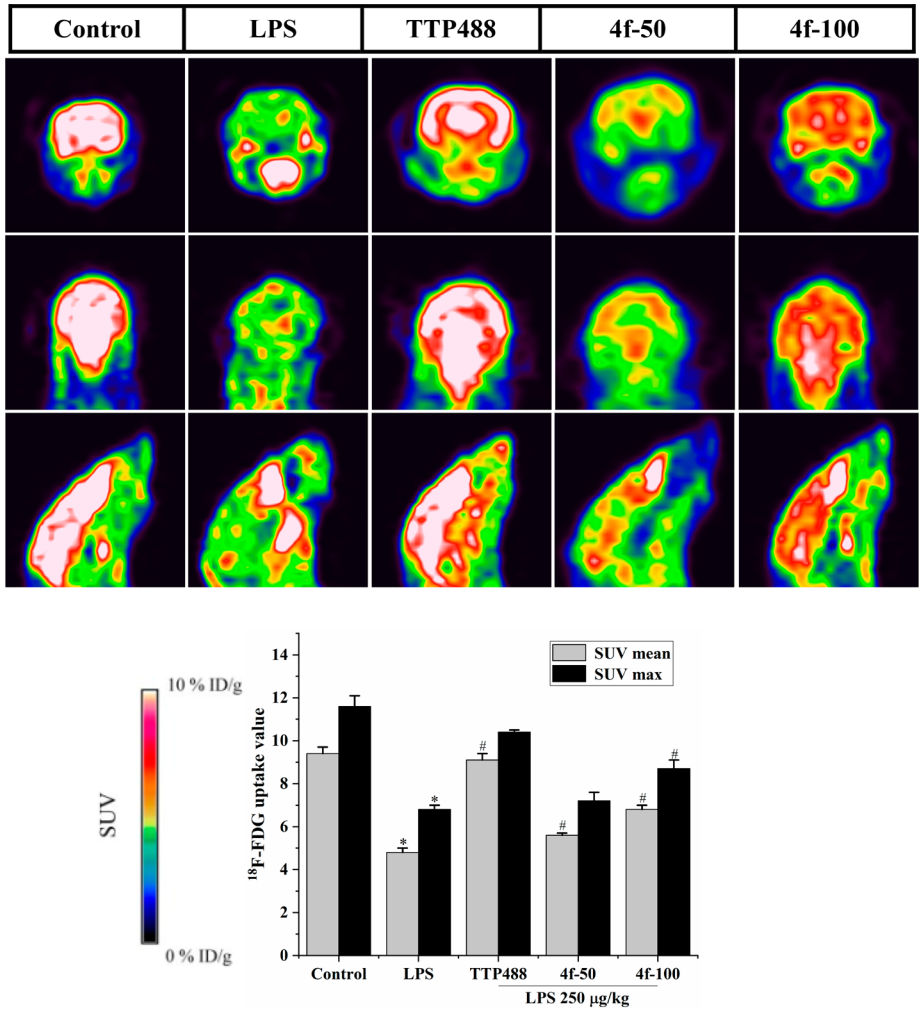

Figure 2. Effects of compound **4f** on LPS-induced cerebral metabolism. Data represent the mean ± SD (n = 6 mice per group). Significantly different from the control group at *p < 0.05; from the LPS group at #p < 0.05.

compound **4f**-treated groups found the platform by a shorter route.

In the spatial probe test, mice from all groups placed in the water maze without the hidden platform were used to assess memory performance. As illustrated in Figure 1C,D, the LPS-treated mice showed significant memory impairment. However, the result was reversed in TTP488 and compound **4f**-treated mice. Furthermore, mice in the TTP488 and compound **4f** groups spent more time in the target quadrant and had greater numbers of platform crossings compared to those of the LPS group. These results also indicated that mice treated with compound **4f** showed dose-dependent increases in the time spent in the target quadrant and crossing times. Additionally, the recorded tracks of the mice from all groups clearly confirmed these results (Figure 1E). LPS, a well-studied immune stimulator, was reported to induce immune neuroinflammatory responses, cause cognitive impairment, and dysregulate glucose metabolism in mice.[31,32] Herein, to assess the relevance of cerebral metabolism in cognitive impairment in mice, we investigated the effects of compound **4f** on brain glucose uptake using an LPS-induced Alzheimer's mouse model. Micro-PET/CT imaging indicated that in mice treated with LPS alone, the uptake of ^{18}F-fluorodeoxyglucose (^{18}F-FDG) in the brain was significantly lower than that in the control group mice (Figure 2). Compound **4f** was also shown to increase ^{18}F-FDG uptake in a dose-dependent manner. Furthermore, mice, treated with TTP488 and compound **4f** (LPS + 100 mg/kg/d), markedly increased neuronal glucose utilization and normalized glucose metabolism. Taken together, these results demonstrated that compound **4f** could reverse memory disturbance and normalize glucose uptake and metabolism in the LPS-induced Alzheimer's mouse model.

To evaluate the effect of compound **4f** on LPS-induced neuron damage, Nissl staining was used to determine the histopathologic changes. As shown in Figure 3, the results demonstrated that LPS treatment resulted in the loss of Nissl substance and dead neurons in the brains compared to the brains of the control group. In contrast, compound **4f** administration markedly elevated Nissl substance in the hippocampus of the mice, increased the number of neurons, and protected normal neurons in the cortex and hippocampus from damage by LPS.

Neuroinflammatory cytokines secreted by activated microglia and astrocytes, which are crucial in neuroinflammatory processes, lead to AD.[13] Thus, the LPS-induced expression of IL-1β in AD mice in the absence or presence of compound **4f** was tested to investigate the effect of compound **4f** on cytokine production. As shown in Figure 4, the marked overexpression of IL-1β was observed in mice treated with LPS compared to the controls. However, pretreatment with different doses of

https://dx.doi.org/10.1021/acschemneuro.0c00578
ACS Chem. Neurosci. 2021, 12, 419−429

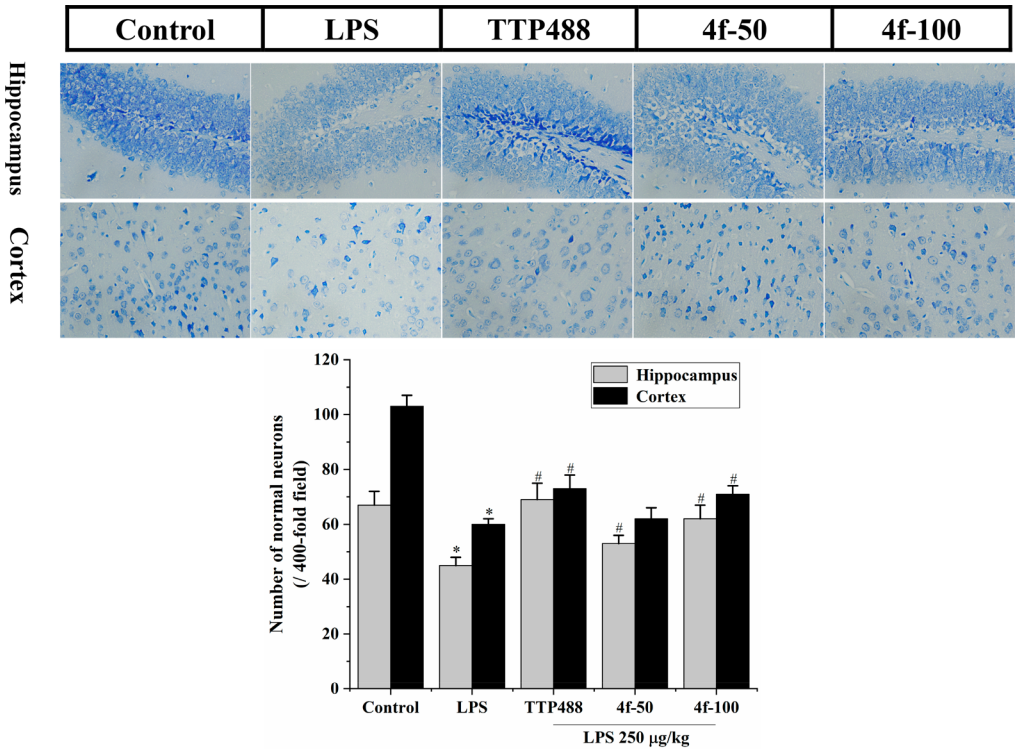

Figure 3. Effects of compound **4f** on normal neurons in the cortex and hippocampus. Nissl staining and normal neuronal counts in the hippocampus and cortex of each group. Scale bar = 50 μm. The data represent the mean ± SD (n = 6 mice per group). Significantly different from the control group at *p < 0.05; from the LPS group at #p < 0.05.

compound **4f** could prevent the cytotoxicity of LPS in the brain. Moreover, IL-1β expression was dose-dependently suppressed by compound **4f**.

When stimulated by LPS, the MAPK and NF-κB signaling pathways were activated and subsequently resulted in the release of proinflammatory cytokines, which were confirmed to be involved in the development of various inflammatory disorders, such as AD.[33] Thus, the antineuroinflammatory mechanisms of action of compound **4f** were investigated by Western blotting. As illustrated in Figure 3, compound **4f** dose-dependently lowered the LPS-induced expression of MAPK p38 and NF-κB p65, whereas treatment with compound **4f** showed no evident effect on the expression of TLR4 and Myd88. Taken together, these results indicated that compound **4f** suppressed LPS-induced IL-1β activation by inhibiting the MAPK/NF-κB signaling pathway.

As described in Figure 5A,B, compound **4f** was docked into the binding pocket of IL-1β (PDB ID: 9ILB). Compound **4f** nested well into the active pocket of IL-1β. Furthermore, the oxygen atom of the OCH_3 group formed a hydrogen bond with SER84 in the catalytic pocket to enhance the affinity for IL-1β.

AD, a neurodegenerative disease, is closely related to aging.[34] A number of studies have indicated that a low-dosage LPS, injection to mice, induced a series of behavioral changes, such as cognitive disorders and memory loss, which well-mimic the symptoms of AD patients.[35] Furthermore, it was demonstrated that α-, β- and γ-secretases, activated by LPS triggered the overexpression of proinflammatory cytokines in the brain and caused physiological symptoms and behavioral symptoms.[36,37] Interestingly, numerous studies confirmed that changes in regional brain metabolism and energetics played a vital role in the pathogenesis of cognitive disorders and memory loss. In addition, it was shown that late-onset AD decreased bilateral glucose metabolism.[38] Therefore, we designed and synthesized cinnamic acid derivatives containing D-amino acids and determined the effects of these compounds *in vitro* and *in vivo*. Moreover, the inhibitory effect of compound **4f** on cerebral glucose metabolism was investigated by micropositron emission tomography (PET) imaging. Additionally, the behavioral experiments clearly demonstrated that compound **4f** effectively attenuated LPS-induced cognitive impairment, such as those on working memory and spatial cognitive memory.

Accumulating evidence has indicated that changes in the structure and function of the pyramidal cells in the hippocampus and cortex were closely implicated in cognitive and behavioral function.[39,40] Herein, we determined the effect of compound **4f** on the LPS-induced pyramidal cells using Nissl staining. The results demonstrated that the LPS injections caused a considerable loss of Nissl-stained cells compared with control group mice. However, cinnamic acid derivative treatment reversed the pathological changes in the hippocampus. Furthermore, compound **4f** inhibited pyramidal cells damage in a dose-dependent manner.

Previous studies indicated that neuroinflammation stimulated by LPS correlated with the overexpression of proinflammatory cytokines, which was confirmed to be one of the causes of neuropathogenesis and cognitive impairment.[41,42] Moreover, LPS, well-known as a TLR4 ligand, led to the initiation of a series of neuroinflammatory cascades, such as the MAPK and NF-κB signaling pathway.[43] Hence, it is necessary to evaluate the inhibitory effect of compound **4f** on LPS-induced inflammatory processes. Our studies revealed that inflammatory responses in the brain of the mice treated with LPS were significantly exacerbated through the release of IL-

https://dx.doi.org/10.1021/acschemneuro.0c00578
ACS Chem. Neurosci. 2021, 12, 419−429

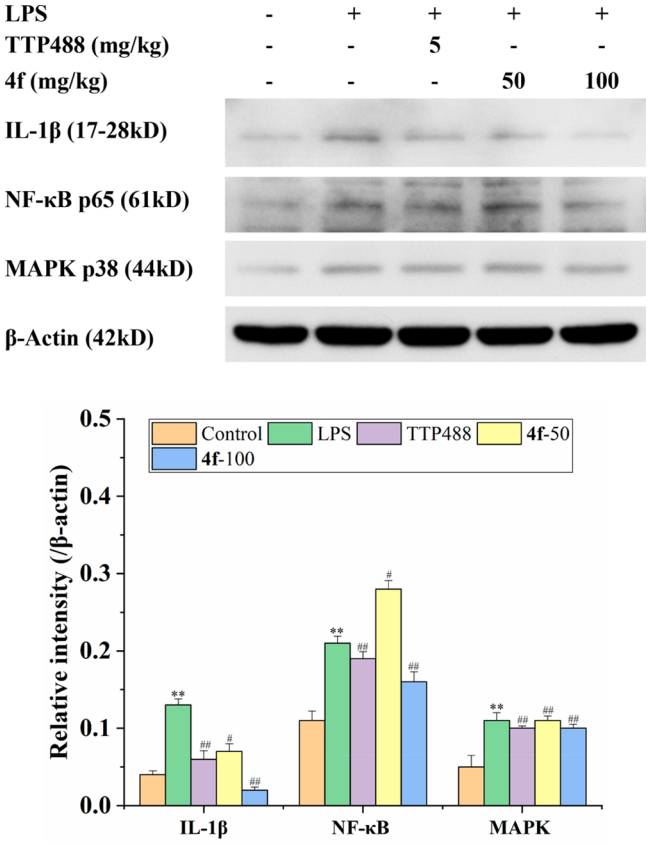

Figure 4. Anti-inflammatory mechanism of compound **4f** against LPS-induced neuroinflammation in mice. Significantly different from the control group at $^{*}p < 0.05$ and $^{**}p < 0.01$; from the LPS group at $^{\#}p < 0.05$ and $^{\#\#}p < 0.01$.

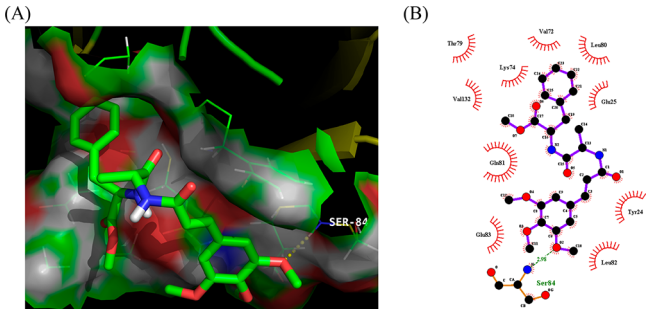

Figure 5. Proposed binding model of the **4f**-IL-1β complex. (A) The yellow dashed lines represent hydrogen bonds. (B) The green dashed lines represent hydrogen bonds.

1β. However, compound **4f** suppressed the release of IL-1β in a dose-dependent manner. In particular, our mechanistic studies demonstrated that the systemic injection of LPS activated MAPK and NF-κB signaling pathways, indicated by the down-regulated expression of IL-1β *in vivo*.

In summary, we demonstrated that novel antineuroinflammatory agents could be discovered by assembling the active fragments of cinnamic acid and D-amino acid. Among the synthesized compounds, compound **4f** significantly inhibited neuroinflammation, and exerted good neuroprotective effects. The *in vitro* and *in vivo* experiments indicated that compound **4f** exerted suppressive effects in LPS-induced neuroinflammation and cognitive impairment by inhibiting the overexpression of IL-1β dependent upon the MAPK-mediated inflammatory signaling pathway. Moreover, a molecular docking study confirmed that compound **4f** could be effectively inserted into the active pocket of IL-1β protein and formed a hydrogen bond with SER84. Collectively, these results demonstrated that compound **4f** could be a promising lead for further optimization as a new antineuroinflammatory agent against Alzheimer's disease.

METHODS

Materials and Methods. LPS (*Escherichia coli* O55:B5) was purchased from Sigma-Aldrich (St. Louis, MO, USA). TTP488, referred to in a previous publication,[44] was used as a standard compound in the experiment. Antibodies against TLR4, Myd88, MAPK p38, NF-κB p65, and IL-1β were obtained from Bioss Biotechnology Co. (Beijing, China). Reagents were used without further purification unless specified. ^{1}H nuclear magnetic resonance (NMR) and ^{13}C NMR spectra were recorded using tetramethylsilane (TMS) as an internal standard on a Bruker DPX-500 spectrometer. Mass spectrometry analysis was performed on a liquid chromatography−mass spectrometer (LC-MS, LCQ) with an ESI source. Melting points were determined on a micro melting point apparatus (Shanghai, China) and were not corrected. Optical rotations were obtained using a WZZ-1S digital polarimeter (Shanghai, China) at sodium D line (589 nm) and were reported in concentrations of 0.01 g/mL.

General Procedure for the Synthesis of Target Compounds. Cinnamic acid (**1a**−**f**) (2.0 mmol, 1 equiv), D-alanine methyl ester hydrochloride (2.0 mmol, 1 equiv), EDC·HCl (2.4 mmol, 1.2 equiv), and HOAt (2.4 mmol, 1.2 equiv) were dissolved in dichloromethane (DCM, 20 mL), and then triethanolamine (TEA, 0.2 mmol, 0.1 equiv) was added slowly. The reaction mixture was stirred at room temperature until the reaction was completed. Then, the reaction mixture was quenched with saturated aqueous $NaHCO_3$ solution and extracted with ethyl acetate. The organic layer was subsequently washed with water and brine, dried over anhydrous Na_2SO_4, and concentrated. The obtained residues were purified by flash chromatography (EtOAc/PE = 1/10) to yield compounds **2a**−**f**. The compounds **2a**−**f** were reacted with LiOH using MeOH/THF/H_2O (3:1:1, 15 mL) as a solvent. After 2 h, 12 M HCl solution was added to the reaction mixture. The solvent was removed under reduced pressure to yield compounds **3a**−**f**.

Compounds **3a**−**f** (1.5 mmol, 1 equiv), D-phenylalanine methyl ester hydrochloride (1.5 mmol, 1 equiv), EDC·HCl (1.8 mmol, 1.2 equiv), and HOAt (1.8 mmol, 1.2 equiv) were dissolved in DCM (20 mL), and TEA (0.15 mmol, 0.1 equiv) was added slowly. The reaction mixture was stirred at room temperature until the reaction was completed. Then the reaction mixture was quenched with saturated aqueous $NaHCO_3$ solution and extracted with ethyl acetate. The organic layer was subsequently washed with water and brine, dried over anhydrous Na_2SO_4, and concentrated. The obtained residues were purified by flash chromatography (EtOAc/PE = 1/5) to provide compounds **4a**−**f**. Compounds **4a**−**f** were reacted with LiOH using MeOH/THF/H_2O (3:1:1, 15 mL) as a solvent. After 2 h, 12 M HCl solution was added to the reaction mixture. The solvent was removed under reduced pressure to provide compounds **5a**−**f**.

*Methyl-cinnamoyl-D-alaninate (**2a**).* This compound is a white solid; yield 89.1%; mp = 119−120 °C; $[\alpha]_D^{21} = -12.0$ (c = 0.5, CH_2Cl_2); ^{1}H NMR (500 MHz, $CDCl_3$): δ 7.57 (d, J = 15.6 Hz, 1H), 7.46−7.41 (m, 2H), 7.03 (t, J = 8.6 Hz, 2H), 6.48 (d, J = 7.2 Hz, 1H), 6.36 (d, J = 15.6 Hz, 1H), 4.78−4.68 (m, 1H), 3.77 (s, 3H), 1.87 (s, 1H), 1.46 (d, J = 7.2 Hz, 3H). ^{13}C NMR (126 MHz, $CDCl_3$): δ 173.82, 165.24, 164.58, 162.59, 140.43, 130.89, 130.87, 129.72, 129.65, 119.78, 119.77, 116.01, 115.84, 52.63, 48.20, 18.54. HRMS calcd for $C_{13}H_{15}NO_3$, $[M - H]^-$ 232.0979, found 232.0972.

*Methyl-(E)-(3-(p-tolyl)acryloyl)-D-alaninate (**2b**).* This compound is a white solid; yield 81.4%; mp = 171−173 °C; $[\alpha]_D^{21} = -13.7$ (c = 0.5, CH_2Cl_2); ^{1}H NMR (500 MHz, $CDCl_3$): δ 7.59 (d, J = 15.6 Hz, 1H), 7.37 (d, J = 8.0 Hz, 2H), 7.15 (d, J = 7.9 Hz, 2H), 6.43 (dd, J = 19.7, 11.4 Hz, 2H), 4.77−4.71 (m, J = 7.2 Hz, 1H), 3.76 (s, 3H), 2.34

https://dx.doi.org/10.1021/acschemneuro.0c00578
ACS Chem. Neurosci. 2021, 12, 419−429

(s, 3H), 1.46 (d, J = 7.2 Hz, 3H). ^{13}C NMR (126 MHz, $CDCl_3$): δ 173.81, 165.62, 141.66, 140.13, 131.90, 129.55, 127.88, 119.00, 52.59, 48.19, 21.45, 18.60. HRMS calcd for $C_{14}H_{17}NO_3$, $[M - H]^-$ 246.1136, found 246.1129.

Methyl-(E)-(3-(4-methoxyphenyl)acryloyl)-D-alaninate (**2c**). This compound is a white solid; yield 83.8%; mp: = 144−146 °C; $[\alpha]_D^{21}$ = −9.1 (c = 0.5, CH_2Cl_2); ^{1}H NMR (500 MHz, $CDCl_3$): δ 7.57 (d, J = 15.6 Hz, 1H), 7.41 (t, J = 5.7 Hz, 2H), 6.89−6.84 (m, 2H), 6.40 (d, J = 7.3 Hz, 1H), 6.32 (d, J = 15.6 Hz, 1H), 4.77−4.71 (m, J = 7.2 Hz, 1H), 3.81 (s, 3H), 3.76 (s, 3H), 1.46 (d, J = 7.2 Hz, 3H). ^{13}C NMR (126 MHz, $CDCl_3$): δ 173.86, 165.75, 160.95, 141.30, 129.47, 127.38, 117.65, 114.23, 77.35, 77.09, 76.84, 55.36, 52.57, 48.16, 18.61. HRMS calcd for $C_{14}H_{17}NO_4$, $[M - H]^-$ 262.1085, found 262.1080.

Methyl-(E)-(3-(4-fluorophenyl)acryloyl)-D-alaninate (**2d**). This compound is a white solid; yield 87.1%; mp = 189−190 °C; $[\alpha]_D^{21}$ = −11.2 (c = 0.5, CH_2Cl_2); ^{1}H NMR (500 MHz, $CDCl_3$): δ 7.57 (d, J = 15.6 Hz, 1H), 7.43−7.40 (m, 2H), 6.87−6.84 (m, 2H), 6.40 (d, J = 7.2 Hz, 1H), 6.33−6.30 (d, J = 15.6 Hz, 1H), 4.77−4.71 (m, 1H), 3.77 (s, 3H), 1.46 (d, J = 7.2 Hz, 3H). ^{13}C NMR (126 MHz, $CDCl_3$): δ 173.82, 165.24, 164.58, 162.59, 140.43, 130.88 (d, J = 3.4 Hz), 129.68 (d, J = 8.6 Hz), 119.78 (d, J = 1.8 Hz), 116.01, 115.84, 52.63, 48.20, 18.54. HRMS calcd for $C_{13}H_{14}FNO_3$, $[M - H]^-$ 250.0885, found 250.0879.

Methyl-(E)-(3-(4-(trifluoromethyl)phenyl)acryloyl)-D-alaninate (**2e**). This compound is a white solid; yield 79.3%; mp = 212−213 °C; $[\alpha]_D^{21}$ = −14.5 (c = 0.5, CH_2Cl_2); ^{1}H NMR (500 MHz, $CDCl_3$): δ 7.63−7.51 (m, 5H), 6.63 (d, J = 7.3 Hz, 1H), 6.52 (d, J = 15.6 Hz, 1H), 4.78−4.72 (m, J = 7.2 Hz, 1H), 3.77 (s, 3H), 1.47 (d, J = 7.2 Hz, 3H). ^{13}C NMR (126 MHz, $CDCl_3$): δ 173.78, 164.77, 139.94, 138.04, 131.41, 131.15, 127.98, 125.77 (d, J = 3.7 Hz), 124.95, 122.79, 122.51, 77.33, 77.07, 76.82, 52.67, 48.28, 18.45. HRMS calcd for $C_{14}H_{14}F_3NO_3$, $[M - H]^-$ 300.0853, found 300.0848.

Methyl-(E)-(3-(3,4,5-trimethoxyphenyl)acryloyl)-D-alaninate (**2f**). This compound is a white solid; yield 83.8%; mp = 137−138 °C; $[\alpha]_D^{21}$ = −13.1 (c = 0.5, CH_2Cl_2); ^{1}H NMR (500 MHz, $CDCl_3$): δ 7.50 (d, J = 15.5 Hz, 1H), 6.68 (s, 2H), 6.47 (d, J = 7.4 Hz, 1H), 6.36 (d, J = 15.5 Hz, 1H), 4.76−4.70 (m, J = 7.2 Hz, 1H), 3.85 (d, J = 1.5 Hz, 9H), 3.76 (s, 3H), 1.45 (d, J = 7.2 Hz, 3H). ^{13}C NMR (126 MHz, $CDCl_3$): δ 173.85, 165.33, 153.33, 141.57, 139.50, 130.26, 119.45, 104.88, 60.96, 56.08, 52.61, 48.17, 18.57. HRMS calcd for $C_{16}H_{21}NO_6$, $[M - H]^-$ 322.1296, found 322.1292.

Cinnamoyl-D-alanine (**3a**). This compound is a white solid; yield 61.5%; mp = 169−171 °C; $[\alpha]_D^{21}$ = −15.1 (c = 0.5, MeOH); ^{1}H NMR (500 MHz, DMSO-d_6): δ 7.68−7.64 (d, J = 7.3 Hz, 1H), 7.48 (t, J = 7.1 Hz, 2H), 7.34 (dd, J = 10.8, 10.3 Hz, 3H), 6.48−6.44 (d, J = 15.9 Hz, 1H), 4.71−4.67 (t, J = 7.3 Hz, 1H), 1.52 (d, J = 7.3 Hz, 3H), 1.25 (s, 1H). ^{13}C NMR (126 MHz, DMSO-d_6): δ 174.63, 165.09, 139.54, 135.34, 129.98, 129.43, 128.00, 122.30, 48.17, 17.86. HRMS calcd for $C_{12}H_{13}NO_3$, $[M - H]^-$ 218.0823, found 218.0815.

(E)-(3-(p-tolyl)acryloyl)-D-alanine (**3b**). Thisc compound is a white solid; yield 54.8%; mp = 240−241 °C; $[\alpha]_D^{21}$ = −12.5 (c = 0.5, MeOH); ^{1}H NMR (500 MHz, DMSO-d_6): δ 8.43 (d, J = 7.3 Hz, 1H), 7.45 (d, J = 8.1 Hz, 2H), 7.39 (d, J = 15.8 Hz, 1H), 7.22 (d, J = 8.0 Hz, 2H), 6.66 (d, J = 15.8 Hz, 1H), 4.35−4.29 (m, J = 7.3 Hz, 1H), 2.31 (s, 3H), 1.31 (d, J = 7.3 Hz, 3H). ^{13}C NMR (126 MHz, DMSO-d_6): δ 174.33, 164.93, 139.41, 139.17, 132.15, 129.67, 127.63, 120.77, 47.74, 21.05, 17.40. HRMS calcd for $C_{13}H_{15}NO_3$, $[M - H]^-$ 232.0979, found 232.0972.

(E)-(3-(4-methoxyphenyl)acryloyl)-D-alanine (**3c**). This compound is a white solid; yield 66.2%; mp = 219−220 °C; $[\alpha]_D^{21}$ = −13.8 (c = 0.5, MeOH); ^{1}H NMR (500 MHz, DMSO-d_6): δ 8.35 (d, J = 7.3 Hz, 1H), 7.56−7.47 (m, 2H), 7.38 (d, J = 15.8 Hz, 1H), 7.01−6.92 (m, 2H), 6.57 (d, J = 15.8 Hz, 1H), 4.32 (t, J = 7.3 Hz, 1H), 3.78 (s, 3H), 1.31 (d, J = 7.3 Hz, 3H). ^{13}C NMR (126 MHz, DMSO-d_6): δ 179.53, 170.18, 165.58, 144.01, 134.34, 132.60, 124.47, 119.62, 60.46, 52.87, 22.60. HRMS calcd for $C_{13}H_{15}NO_4$, $[M - H]^-$ 248.0928, found 248.0923.

(E)-(3-(4-fluorophenyl)acryloyl)-D-alanine (**3d**). This compound is a white solid; yield 70.1%; mp = 233−234 °C; $[\alpha]_D^{21}$ = −12.1 (c = 0.5, MeOH); ^{1}H NMR (500 MHz, DMSO-d_6): δ 8.44 (d, J = 7.3 Hz, 1H), 7.65−7.60 (m, 2H), 7.43 (d, J = 15.8 Hz, 1H), 7.25 (t, J = 8.8 Hz, 2H), 6.66 (d, J = 15.8 Hz, 1H), 4.35−4.29 (m, J = 7.3 Hz, 1H), 1.32 (d, J = 7.3 Hz, 3H). ^{13}C NMR (126 MHz, DMSO-d_6): δ 174.67, 165.05, 164.17, 162.20, 138.38, 131.92 (d, J = 2.8 Hz), 130.17 (d, J = 8.5 Hz), 122.08, 116.50, 116.32, 48.15, 17.80. HRMS calcd for $C_{12}H_{12}FNO_3$, $[M - H]^-$ 236.0728, found 236.0721.

(E)-(3-(4-(trifluoromethyl)phenyl)acryloyl)-D-alanine (**3e**). This compound is a white solid; yield 71.9%; mp = 258−260 °C; $[\alpha]_D^{21}$ = −10.9 (c = 0.5, MeOH); ^{1}H NMR (500 MHz, -d_6): δ 8.55 (d, J = 7.3 Hz, 1H), 7.85−7.73 (m, 1H), 7.52 (d, J = 15.9 Hz, 1H), 6.86 (d, J = 15.9 Hz, 1H), 4.37−4.32 (m, J = 7.3 Hz, 1H), 1.34 (d, J = 7.3 Hz, 1H). ^{13}C NMR (126 MHz, DMSO-d_6): δ 174.55, 164.64, 139.39, 137.90, 129.84, 129.59, 128.64, 126.30 (d, J = 3.8 Hz), 125.65, 125.03, 123.49, 48.23, 17.78. HRMS calcd for $C_{13}H_{12}F_3NO_3$, $[M - H]^-$ 286.0697, found 286.0693.

(E)-(3-(3,4,5-trimethoxyphenyl)acryloyl)-D-alanine (**3f**). Light yellow solid; yield 67.2%; mp = 196−198 °C; $[\alpha]_D^{21}$ = −13.5 (c = 0.5, CH_2Cl_2); ^{1}H NMR (500 MHz, DMSO): δ 8.32 (d, J = 7.3 Hz, 1H), 7.37 (d, J = 15.7 Hz, 1H), 6.90 (s, 2H), 6.67 (d, J = 15.8 Hz, 1H), 4.32 (t, J = 7.3 Hz, 1H), 3.81 (s, 6H), 3.68 (s, 3H), 1.32 (d, J = 7.3 Hz, 3H). ^{13}C NMR (126 MHz, DMSO): δ 174.68, 165.19, 153.53, 139.65, 139.10, 130.95, 121.65, 105.34, 60.54, 56.29, 48.11, 17.82. HRMS calcd for $C_{15}H_{19}NO_6$, $[M - H]^-$ 308.1140, found 308.1136.

Methyl-cinnamoyl-D-alanyl-D-phenylalaninate (**4a**). This compound is a white solid; yield 80.4%; mp = 160−161 °C; $[\alpha]_D^{21}$ = +19.9 (c = 0.5, CH_2Cl_2); ^{1}H NMR (400 MHz, $CDCl_3$): δ 7.63 (d, J = 15.7 Hz, 1H), 7.48 (dd, J = 6.5, 2.9 Hz, 2H), 7.36−7.28 (m, 4H), 7.23−7.18 (m, 2H), 7.13 (dd, J = 8.8, 5.8 Hz, 1H), 7.09 (s, 1H), 6.97 (d, J = 7.7 Hz, 1H), 6.50 (d, J = 15.7 Hz, 1H), 4.86 (dd, J = 13.8, 6.8 Hz, 1H), 4.78 (d, J = 7.3 Hz, 3H), 3.14 (dd, J = 13.8, 5.8 Hz, 1H), 3.05 (dd, J = 13.8, 6.9 Hz, 1H), 1.42 (d, J = 7.0 Hz, 3H). ^{13}C NMR (126 MHz, $CDCl_3$): δ 172.35, 171.75, 165.43, 140.21, 135.69, 133.21, 129.36, 128.61, 127.12, 120.78, 53.52, 52.43, 48.81, 37.89, 18.44. HRMS calcd for $C_{22}H_{24}N_2O_4$, $[M - H]^-$ 379.1663, found 379.1659.

Methyl-((E)-3-(p-tolyl)acryloyl)-D-alanyl-D-phenylalaninate (**4b**). This compound is a white solid; yield 88.6%; mp = 125−126 °C; $[\alpha]_D^{21}$ = +16.2 (c = 0.5, CH_2Cl_2); ^{1}H NMR (500 MHz, $CDCl_3$): δ 7.60 (d, J = 15.6 Hz, 1H), 7.40 (d, J = 8.0 Hz, 2H), 7.22 (t, J = 7.2 Hz, 2H), 7.17 (d, J = 7.6 Hz, 3H), 7.11−7.07 (m, 2H), 6.90 (s, 1H), 6.37 (dd, J = 15.5, 8.0 Hz, 2H), 4.90−4.81 (m, 1H), 4.65 (dd, J = 12.3, 5.1 Hz, 1H), 3.72 (d, J = 11.0 Hz, 3H), 3.15 (dd, J = 14.0, 5.6 Hz, 1H), 3.05 (dd, J = 13.9, 6.8 Hz, 1H), 2.37 (s, 2H), 1.39 (d, J = 7.0 Hz, 3H). ^{13}C NMR (126 MHz, $CDCl_3$): δ 172.02, 171.72, 165.87, 141.78, 140.26, 135.73, 131.87, 129.64, 129.27, 128.62, 127.89, 127.10, 118.94, 53.39, 52.45, 48.71, 37.88, 21.49, 18.12. HRMS calcd for $C_{23}H_{26}N_2O_4$, $[M - H]^-$ 393.1820, found 393.1817.

Methyl-((E)-3-(4-methoxyphenyl)acryloyl)-D-alanyl-D-phenylalaninate (**4c**). This compound is a white solid; yield 85.1%; mp = 147−149 °C; $[\alpha]_D^{21}$ = +21.7 (c = 0.5, CH_2Cl_2); ^{1}H NMR (500 MHz, $CDCl_3$): δ 7.58 (d, J = 15.6 Hz, 1H), 7.44 (dd, J = 8.6, 3.9 Hz, 2H), 7.20 (d, J = 7.5 Hz, 2H), 7.17−7.13 (m, 1H), 7.09 (d, J = 7.0 Hz, 2H), 7.04 (d, J = 8.0 Hz, 1H), 6.87 (d, J = 8.7 Hz, 2H), 6.49 (d, J = 7.6 Hz, 1H), 6.30 (dd, J = 15.6, 5.5 Hz, 1H), 4.84 (dd, J = 13.6, 6.7 Hz, 1H), 4.67 (dd, J = 14.7, 7.4 Hz, 1H), 3.82 (s, 3H), 3.71 (d, J = 10.4 Hz, 3H), 3.14 (dd, J = 13.8, 5.6 Hz, 1H), 3.06−3.00 (m, 1H), 1.39 (d, J = 7.0 Hz, 3H). ^{13}C NMR (126 MHz, $CDCl_3$): δ 172.21, 171.75, 166.07, 161.02, 141.38, 135.79, 129.50, 129.28, 128.60, 127.37, 127.07, 117.65, 114.30, 55.38, 53.44, 52.43, 48.70, 37.89, 18.15. HRMS calcd for $C_{23}H_{26}N_2O_5$, $[M - H]^-$ 409.1769, found 409.1765.

Methyl-((E)-3-(4-fluorophenyl)acryloyl)-D-alanyl-D-phenylalaninate (**4d**). This compound is a white solid; yield 75.6%; mp = 173−175 °C; $[\alpha]_D^{21}$ = +15.0 (c = 0.5, CH_2Cl_2); ^{1}H NMR (500 MHz, DMSO-d_6): δ 8.45 (d, J = 7.6 Hz, 1H), 8.28 (d, J = 7.8 Hz, 1H), 7.66−7.59 (m, 2H), 7.44 (d, J = 15.8 Hz, 1H), 7.31−7.25 (m, 4H), 7.25−7.18 (m, 3H), 6.71 (d, J = 15.8 Hz, 1H), 4.55−4.43 (m, 2H), 3.61 (d, J = 20.3 Hz, 3H), 3.05 (dd, J = 13.9, 5.7 Hz, 1H), 2.97−2.90 (m, 1H), 1.23 (d, J = 7.1 Hz, 3H). ^{13}C NMR (126 MHz, DMSO-d_6): δ 172.88, 172.29, 164.87, 164.14, 162.18, 138.21, 137.55, 132.02, 130.13 (d, J = 8.4 Hz), 129.63 (d, J = 14.1 Hz), 128.68 (d, J = 10.4

https://dx.doi.org/10.1021/acschemneuro.0c00578
ACS Chem. Neurosci. 2021, 12, 419−429

Hz), 127.02, 122.36, 116.49, 116.32, 54.08, 52.33, 48.32, 36.97, 18.86. HRMS calcd for $C_{22}H_{23}FN_2O_4$, $[M - H]^-$ 397.1569, found 397.1565.

*Methyl-(E)-(2-(3-(4-(trifluoromethyl)phenyl)acrylamido)-acryloyl)-D-phenylalaninate (**4e**).* This compound is a white solid; yield 80.2%; mp = 191−192 °C; $[\alpha]_D^{21}$ = +19.7 (*c* = 0.5, CH_2Cl_2); ^{1}H NMR (500 MHz, $CDCl_3$): δ 7.64 (s, 1H), 7.62−7.55 (m, 5H), 7.24−7.20 (m, 2H), 7.17 (ddd, *J* = 7.4, 3.6, 1.3 Hz, 1H), 7.11−7.07 (m, 2H), 6.92 (d, *J* = 8.0 Hz, 1H), 6.74 (d, *J* = 7.6 Hz, 1H), 6.51 (d, *J* = 15.6 Hz, 1H), 4.87 (dt, *J* = 7.8, 6.2 Hz, 1H), 4.70 (dd, *J* = 14.5, 7.2 Hz, 1H), 3.72 (d, *J* = 7.2 Hz, 3H), 3.15 (dd, *J* = 13.9, 5.7 Hz, 1H), 3.07 (dd, *J* = 13.9, 6.5 Hz, 1H), 1.42 (d, *J* = 7.0 Hz, 3H). ^{13}C NMR (126 MHz, $CDCl_3$): δ 172.05, 171.68, 164.97, 139.93, 138.09, 135.63, 129.26, 128.64, 127.99, 127.17, 125.85 (d, *J* = 3.7 Hz), 122.60, 53.44, 52.47, 48.88, 37.88, 18.44. HRMS calcd for $C_{23}H_{23}F_3N_2O_4$, $[M - H]^-$ 447.1537, found 447.1534.

*Methyl-((E)-3-(3,4,5-trimethoxyphenyl)acryloyl)-D-alanyl-D-phenylalanin-eate (**4f**).* This compound is a white solid; yield 84.5%; mp = 183−184 °C; $[\alpha]_D^{21}$ = +17.6 (*c* = 0.5, CH_2Cl_2); ^{1}H NMR (500 MHz, $CDCl_3$): δ 7.56 (d, *J* = 15.5 Hz, 1H), 7.31−7.23 (m, 3H), 7.22−7.17 (m, 1H), 7.12 (d, *J* = 6.8 Hz, 2H), 6.96 (d, *J* = 7.9 Hz, 1H), 6.74 (d, *J* = 2.6 Hz, 2H), 6.52 (d, *J* = 7.6 Hz, 1H), 6.36 (d, *J* = 15.5 Hz, 1H), 4.89−4.82 (m, 1H), 4.70 (dd, *J* = 14.1, 6.8 Hz, 1H), 3.89 (t, *J* = 2.3 Hz, 9H), 3.74 (d, *J* = 6.9 Hz, 3H), 3.17 (dd, *J* = 13.9, 5.7 Hz, 1H), 3.08 (dd, *J* = 13.8, 6.6 Hz, 1H), 1.42 (d, *J* = 7.0 Hz, 3H). ^{13}C NMR (126 MHz, $CDCl_3$): δ 172.10, 171.72, 165.57, 153.40, 141.68, 139.61, 135.72, 130.23, 129.27, 128.62, 127.12, 119.42, 104.92, 61.00, 56.11, 53.44, 52.44, 48.77, 37.90, 18.39. HRMS calcd for $C_{25}H_{30}N_2O_7$, $[M - H]^-$ 469.1980, found 469.1974.

*Cinnamoyl-D-alanyl-D-phenylalanine (**5a**).* This compound is a white solid; yield 72.0%; mp = 203−204 °C; $[\alpha]_D^{21}$ = +18.6 (*c* = 0.5, MeOH); ^{1}H NMR (500 MHz, DMSO): δ 8.31 (d, *J* = 7.8 Hz, 1H), 8.21 (s, 1H), 7.56 (d, *J* = 7.1 Hz, 2H), 7.45−7.39 (m, 3H), 7.39−7.35 (m, 1H), 7.26−7.21 (m, 5H), 7.18−7.13 (m, 1H), 6.77 (d, *J* = 15.8 Hz, 1H), 4.42 (ddd, *J* = 13.4, 11.7, 6.2 Hz, 2H), 3.06 (dd, *J* = 13.8, 5.0 Hz, 1H), 2.94−2.89 (m, 1H), 1.21 (d, *J* = 7.1 Hz, 3H). ^{13}C NMR (126 MHz, DMSO): δ 173.20, 172.64, 164.95, 139.37, 137.99, 135.38, 129.95, 129.67, 129.43, 128.61, 127.99, 126.85, 122.52, 53.98, 48.45, 37.03, 18.83. HRMS calcd for $C_{21}H_{22}N_2O_4$, $[M - H]^-$ 365.1507, found 365.1501.

*((E)-3-(p-tolyl)acryloyl)-D-alanyl-D-phenylalanine (**5b**).* This compound is a white solid; yield 74.1%; mp = 220−221 °C; $[\alpha]_D^{21}$ = +15.0 (*c* = 0.5, MeOH); ^{1}H NMR (500 MHz, DMSO-d_6): δ 8.34 (d, *J* = 7.8 Hz, 1H), 8.25 (d, *J* = 7.9 Hz, 1H), 7.45 (d, *J* = 8.1 Hz, 2H), 7.37 (d, *J* = 15.8 Hz, 1H), 7.24 (s, 1H), 7.23 (d, *J* = 3.0 Hz, 4H), 7.21 (s, 1H), 7.20−7.15 (m, 1H), 6.71 (d, *J* = 15.8 Hz, 1H), 4.53−4.38 (m, 2H), 3.05 (dd, *J* = 13.8, 5.0 Hz, 1H), 2.92 (dd, *J* = 13.8, 9.0 Hz, 1H), 2.31 (s, 3H), 1.20 (d, *J* = 7.1 Hz, 3H). ^{13}C NMR (126 MHz, DMSO-d_6): δ 173.17, 172.74, 165.17, 139.74, 139.37, 137.91, 132.57, 130.03, 129.67, 128.63, 127.98, 126.88, 121.40, 53.94, 48.45, 36.97, 21.42, 18.75. HRMS calcd for $C_{22}H_{24}N_2O_4$, $[M - H]^-$ 379.1663, found 379.1658.

*((E)-3-(4-methoxyphenyl)acryloyl)-D-alanyl-D-phenylalanine (**5c**).* This compound is a white solid; yield 65.6%; $[\alpha]_D^{21}$ = +16.3 (*c* = 0.5, MeOH); mp = 198−199 °C; ^{1}H NMR (500 MHz, DMSO-d_6): δ 12.81 (s, 1H), 8.22 (d, *J* = 7.9 Hz, 1H), 8.18 (d, *J* = 7.8 Hz, 1H), 7.54−7.48 (m, 2H), 7.38 (d, *J* = 15.7 Hz, 1H), 7.28−7.22 (m, 4H), 7.19 (dd, *J* = 6.2, 2.5 Hz, 1H), 6.98 (dd, *J* = 9.0, 2.5 Hz, 2H), 6.61 (d, *J* = 15.8 Hz, 1H), 4.57−4.30 (m, 2H), 3.78 (d, *J* = 1.8 Hz, 3H), 3.10−2.99 (m, 1H), 2.91 (d, *J* = 8.8 Hz, 1H), 1.22 (d, *J* = 7.1 Hz, 3H). ^{13}C NMR (126 MHz, DMSO-d_6): δ 173.23, 172.75, 165.28, 160.80, 139.13, 137.92, 129.65, 129.57, 128.64, 127.93, 126.88, 119.97, 114.87, 55.71, 53.91, 48.34, 37.03, 18.83. HRMS calcd for $C_{22}H_{24}N_2O_5$, $[M - H]^-$ 395.1612, found 395.1607.

*((E)-3-(4-fluorophenyl)acryloyl)-D-alanyl-D-phenylalanine (**5d**).* This compound is a white solid; yield 70.9%; mp = 217−219 °C; $[\alpha]_D^{21}$ = +18.2 (*c* = 0.5, MeOH); ^{1}H NMR (500 MHz, DMSO-d_6): δ 8.37 (dd, *J* = 11.8, 8.2 Hz, 1H), 8.29 (dd, *J* = 25.5, 7.9 Hz, 1H), 7.62 (ddd, *J* = 8.6, 5.4, 2.9 Hz, 2H), 7.41 (d, *J* = 15.8 Hz, 1H), 7.28 (t, *J* = 6.3 Hz, 1H), 7.26−7.24 (m, 2H), 7.23 (d, *J* = 3.6 Hz, 3H), 7.17 (dd, *J* = 8.5, 4.1 Hz, 1H), 6.73 (d, *J* = 15.8 Hz, 1H), 4.51−4.33 (m, 2H), 3.11−2.99 (m, 1H), 2.95−2.78 (m, 1H), 1.21 (d, *J* = 7.1 Hz, 3H), 1.03 (d, *J* = 7.1 Hz, 1H). ^{13}C NMR (126 MHz, DMSO-d_6): δ 173.17, 172.69, 164.93, 138.18, 137.94, 130.15 (d, *J* = 8.4 Hz), 129.67, 128.62, 126.87, 122.38, 116.50, 116.32, 53.98, 48.49, 36.97, 18.79. HRMS calcd for $C_{21}H_{21}FN_2O_4$, $[M - H]^-$ 383.1413, found 383.1405.

*((E)-3-(4-(trifluoromethyl)phenyl)acryloyl)-D-alanyl-D-phenylalanine (**5e**).* This compound is a white solid; yield 69.1%; mp = 226−227 °C; $[\alpha]_D^{21}$ = +17.3 (*c* = 0.5, MeOH); ^{1}H NMR (500 MHz, DMSO-d_6): δ 8.44−8.35 (m, 1H), 8.28 (d, *J* = 7.9 Hz, 1H), 7.82−7.74 (m, 3H), 7.49 (d, *J* = 15.9 Hz, 1H), 7.27−7.20 (m, 4H), 7.18 (td, *J* = 5.9, 2.6 Hz, 1H), 6.91 (d, *J* = 15.9 Hz, 1H), 4.50−4.39 (m, 2H), 3.07 (dd, *J* = 13.8, 4.9 Hz, 1H), 2.92 (dd, *J* = 13.8, 9.0 Hz, 1H), 1.23 (d, *J* = 7.0 Hz, 3H). ^{13}C NMR (126 MHz, DMSO-d_6): δ ^{13}C NMR (126 MHz, DMSO) δ 173.21, 172.56, 164.44, 137.97, 137.69, 129.65, 128.62 (d, *J* = 2.8 Hz), 126.88, 126.33, 125.31, 53.97, 48.46, 36.99, 18.87. HRMS calcd for $C_{22}H_{21}F_3N_2O_4$, $[M - H]^-$ 433.1381, found 433.1373.

*((E)-3-(3,4,5-trimethoxyphenyl)acryloyl)-D-alanyl-D-phenylalanine (**5f**).* This compound is a light yellow solid; yield 77.2%; mp = 185−187 °C; $[\alpha]_D^{21}$ = +13.3 (*c* = 0.5, CH_2Cl_2); ^{1}H NMR (500 MHz, DMSO-d_6): δ 12.77 (s, 1H), 8.22 (d, *J* = 7.9 Hz, 1H), 8.11 (d, *J* = 7.8 Hz, 1H), 7.35 (d, *J* = 15.7 Hz, 1H), 7.26 (d, *J* = 7.4 Hz, 1H), 7.23 (dd, *J* = 5.3, 3.0 Hz, 3H), 7.19 (d, *J* = 6.9 Hz, 1H), 6.90 (d, *J* = 3.7 Hz, 2H), 6.72 (d, *J* = 15.7 Hz, 1H), 4.48−4.37 (m, 2H), 3.80 (d, *J* = 2.0 Hz, 6H), 3.68 (d, *J* = 1.5 Hz, 3H), 3.06 (dd, *J* = 13.9, 5.0 Hz, 1H), 2.91 (dd, *J* = 13.8, 8.9 Hz, 1H), 1.21 (d, *J* = 7.0 Hz, 3H). ^{13}C NMR (126 MHz, DMSO-d_6): δ 164.97, 153.52, 137.91, 131.03, 129.65, 128.65, 126.91, 121.92, 105.29, 60.55, 56.27, 53.87, 48.37, 37.03, 18.95. HRMS calcd for $C_{24}H_{28}N_2O_7$, $[M + H]^+$ 457.1956, found 457.1959.

Cell Culture. Murine microglial (BV-2) cells (Cell Resource Center of Chinese Academy of Medical Science, Beijing, China) were grown in Dulbecco Modified Eagle Medium (DMEM; Gibco, CA, USA) containing 10% fetal bovine serum (FBS, Hyclone, CA, USA) and 1% penicillin/streptomycin (Hyclone, CA, USA) in a 37 °C humidified atmosphere containing 5% CO_2. These cells were subcultured every two days.

NO Production in LPS-Induced BV2 Microglial Cells. NO production was determined by a colorimetric method using the Griess reagent as previously described.[45] Briefly, the BV2 cells were preincubated for 30 min in the absence or presence of all compounds at different concentrations before adding LPS (1 μg/mL, 10 μL) for 24 h at 37 °C. The cell medium was centrifuged, and the supernatant (50 μL) was dispensed into 96-well plates and then mixed with an equal volume of Griess reagent (Beyotime Biotechnology, Beijing, China). The plates were incubated at room temperature for 10 min, and the absorbance at 540 nm was measured using a multifunctional microplate reader. The inhibition rate of NO production was calculated by the following equation:

$$\text{inhibition rate (\%)} = (A_{\text{LPS}} - A_{\text{Compound}})/(A_{\text{LPS}} - A_{\text{Control}}) \times 100\%$$

where A_{Conpound} was the absorbance of the BV2 cells treated with target compounds and LPS, A_{LPS} was the absorbance of the BV2 cells treated with LPS alone, and A_{Control} was the absorbance of normal BV2 cells.

Animals and Comound 4f Treatment. Female C57 mice (5−6 weeks) were obtained from the Center of Animal Testing of Southern Medical University (SCXK/20160041, Guangzhou, China). All animals were randomly divided into five groups with six mice in each group and housed (25 ± 1 °C at 50% relative humidity) under 12 h/12 h light−dark cycle conditions. Food and water were provided *ad libitum*. All animal care and experimental procedures were carried out in strict accordance with the National Institute of Health's Guide for the Care and Use of Laboratory Animals.

As previously published,[46] the LPS-induced Alzheimer's disease model was established as follows:

(1) Control group: Mice in control group were injected with phosphate-buffered saline (PBS) once daily for 14 days.

https://dx.doi.org/10.1021/acschemneuro.0c00578
ACS Chem. Neurosci. 2021, 12, 419−429

(2) LPS group: Mice in the LPS group were injected with PBS once daily for 7 days. After 7 days, the mice were intraperitoneally (i.p.) administered LPS (250 μg/kg) once daily for 7 days after PBS treatment.
(3) TTP488 group: Mice in the TTP488 group were injected with TTP488 (5 mg/kg) once daily for 7 days. After 7 days, the mice were administered LPS (250 μg/kg) i.p. once daily for 7 days after TTP488 (5 mg/kg) treatment.
(4) **4f**-50 group: Mice in the **4f**-50 group were orally administered compound **4f** (50 mg/kg) once daily for 7 days. After 7 days, the mice were administered LPS (250 μg/kg) i.p. once daily for 7 days after compound **4f** (50 mg/kg) treatment.
(5) **4f**-100 group: Mice in the **4f**-100 group were orally administered compound **4f** (100 mg/kg) once daily for 7 days. After 7 days, the mice were administered LPS (250 μg/kg) i.p. once daily for 7 days after compound **4f** (100 mg/kg) treatment.

Micropositron Emission Tomography/Computed Tomography Imaging. The change in brain glucose uptake was determined as previously described.[46] Briefly, after 2 weeks of drug administration, PET scans and image analysis were used to determine brain glucose uptake by compound **4f** in mice in each group. First, after fasting for 12 h, the mice were injected i.p. with ^{18}F-FDG under general anesthesia with 7% chloral hydrate. Ten-minute static PET scans of the mice were obtained 1 h after ^{18}F-FDG injections, followed by a low-dose CT scan (for attenuation correction and localization) using an Inveon Micro-PET/CT system (Siemens Healthiness, Munich, Germany). Second, the images were reconstructed using the Micro-PET/CT manager (Siemens Medical Solutions Inc., Pittsfield, USA) with an attenuation correction. A region-of-interest (ROI), placed on the inflammatory brains, was drawn and measured using Inveon Research Workplace software. Quantification of the ^{18}F-FDG uptake in the brains of each group was calculated to obtain the image-ROI-derived percent injected dose per gram (% ID/g).

Morris Water Maze Test. The behavioral assessment after 2 weeks of drug administration was carried out using MWM as reported earlier.[46] The water maze consisted of a circular pool with a diameter of 120 cm and a hidden platform (1 cm under the water) with a diameter of 10 cm. The pool was filled with opaque water (titanium white powder was added to the water, to enable distinguishing of the black C57 mice) at a temperature of 24 ± 1 °C. A video camera, connected to the SMART video-tracking and analysis system (TSE, Bad Homburg, Germany), was located above the pool and used to track the animal's movement. The MWM test consisted of 4 days of training, 1 day of navigation testing, and 1 day of spatial probe testing. During the 4 days, the hidden platform was kept constant at the midpoint of target quadrant and the mice were trained in the MWM twice daily. The training consisted of four sessions of trials (one session/day, one trial/session). Each trial was performed for 60 s until the mouse climbed onto the hidden platform target. In the navigation test, the mice were free to swim in the pool for 120 s to locate the platform. The escape latency time (s) to find the hidden platform and the time spent in the target quadrant (s) were recorded. During the probe trials, the platform in the quadrant was removed and the mice were put into the pool and swam for 120 s. The mice were monitored with the camera and the percentage (%) of time spent in each quadrant and the number of times the mice crossed the platform area were recorded using the video-tracking and analysis system.

Nissl Staining. The brains of mice from all groups were removed *in toto*, washed twice with 0.01 M PBS, and postfixed in 4% paraformaldehyde (PFA). Paraffin-embedded brain specimens were sectioned coronally (4 μm). For the detection of normal neurons, tissue slices were washed with xylene for 5 min, progressively dehydrated in 100% alcohol and 75% alcohol, consequently stained with a warmed 0.1% toluidine blue solution for 3−5 min, and finally rinsed with distilled water. The slides were imaged and captured using an Olympus confocal microscope (IX-73, Tokyo, Japan). Normal neurons had prominent Nissl granules and a light nucleus and were examined with a 400× objective. The analysis of normal neuronal cells was conducted on three nonoverlapping fields per slice.

Western Blotting. A total of 20 mg of brain proteins from each group was subjected to sodium dodecyl sulfate−polyacrylamide gel electrophoresis (SDS-PAGE) and transferred to nitrocellulose membranes. Immunoblotting was performed using anti-IL-1β (1:5000; WB Preferred), NF-κB p65 (1:5000), and MAPK p38 (1:5000). Immunodetection was done using an enhanced chemiluminescence detection kit (MultiSciences Biotech, Hangzhou, China). The band density was quantified using Quantity One analysis software (Bio-Rad, Hercules, CA, USA) by calculating the average optical density in each field.

Molecular Modeling. AutoDock4.2 was used to simulate the interaction between compound **4f** and IL-1β. After hydrogen atoms were added to compound **4f** using Babel and partial charges were generated using MOPAC, the hydrogen bonding energy of compound **4f** was minimized using the Lenard-Jones 6/12 potential mode and optimized with iterative minimization. In addition, a maximum of 300 iterations was used to optimize the energy gradient, and a total of 200 docking runs were performed in each cycle of the iterative minimization. The crystal structure of IL-1β was retrieved from the RCSB Protein Data Bank (PDB: 9ILB). All water molecules were removed, and hydrogen atoms were added to achieve IL-1β protein protonation. The active pocket of IL-1β protein was simulated by the automatic mode. Other settings were used in the default settings.

Statistical Analysis. The quantitative data are expressed as the mean ± standard deviation (SD). Statistical analysis of the data was performed using Graph Pad Prism 5 software (La Jolla, CA, USA) for comparisons using the Student's *t*-test or one- or two-way ANOVA to determine statistical significance. The *p* values of <0.05 and <0.01 were considered to indicate statistically significant differences.

■ ASSOCIATED CONTENT

Supporting Information

The Supporting Information is available free of charge at https://pubs.acs.org/doi/10.1021/acschemneuro.0c00578.

Experimental Section with ^{1}H and ^{13}C NMR spectra of **2a−5f** and HRMS spectra of **2a−5f** (PDF)

■ AUTHOR INFORMATION

Corresponding Author

Wenfeng Liu − *School of Biotechnology and Health Sciences, Wuyi University, Jiangmen 529020, China; International Healthcare Innovation Institute (Jiangmen), Jiangmen 529020, China;* orcid.org/0000-0002-7169-843X; Email: wyuchemlwf@126.com

Authors

Shun Huang − *Nanfang PET Center, Nanfang Hospital, Southern Medical University, Guangzhou, Guangdong 510515, China*

Yonglian Li − *School of Eco-environment Technology, Guangdong Industry Polytechnic, Guangzhou 510300, China*

Kun Zhang − *School of Biotechnology and Health Sciences, Wuyi University, Jiangmen 529020, China*

Xi Zheng − *School of Biotechnology and Health Sciences, Wuyi University, Jiangmen 529020, China; Susan Lehman Cullman Laboratory for Cancer Research, Department of Chemical Biology, Ernest Mario School of Pharmacy, Rutgers, The State University of New Jersey, Piscataway, New Jersey 08854, United States*

Hubing Wu − *Nanfang PET Center, Nanfang Hospital, Southern Medical University, Guangzhou, Guangdong 510515, China*

Ganghua Tang − *Nanfang PET Center, Nanfang Hospital, Southern Medical University, Guangzhou, Guangdong 510515, China*

https://dx.doi.org/10.1021/acschemneuro.0c00578
ACS Chem. Neurosci. 2021, 12, 419−429

Complete contact information is available at: https://pubs.acs.org/10.1021/acschemneuro.0c00578

Author Contributions

S.H. and W.F.L. conceived the study. Y.L.L. and W.F.L. designed and performed the target compounds. S.H. and W.F.L. designed and performed experiments. X.Z., K.Z., H.B.W., G.H.T., S.H., and W.F.L. analyzed and interpreted data. S.H. and W.F.L. wrote the manuscript.

Funding

Financial support was provided by Natural Science Foundation of Guangdong-Guangzhou Joint Fund (No.: 2019A1515110941), National Natural Science Foundation of China (No.: 81901781), Foundation for Young Talents (No.: 2016KQNCX174, 2017GkQNCX006, and 2017KTSCX184), Foundation for Department of Education of Guangdong Province (No.: 2017KSYS010), President Foundation Project of Nanfang Hospital, Southern Medical University (No.: 2018Z003), the Basic and Theoretical Research Programs of Science and Technology Foundation of Jiangmen (No.: 2020JC01013), and the Joint Fund of Wuyi University-Macau (No.: 2019WGALH01).

Notes

The authors declare no competing financial interest.

REFERENCES

(1) Alzheimer, A. (1911) Über eigenartige krankheitsfälle des späteren alters. *Z. Gesamte Neurol. Psychiatr. 4* (1), 356.

(2) Heneka, M. T., Carson, M. J., El Khoury, J., Landreth, G. E., Brosseron, F., Feinstein, D. L., Jacobs, A. H., Wysscoray, T., Vitorica, J., Ransohoff, R. M., Herrup, K., Frautschy, S. A., Finsen, B., Brown, G. C., Verkhratsky, A., Yamanaka, K., Koistinaho, J., Latz, E., Halle, A., Petzold, G. C., Town, T., Morgan, D., Shinohara, L., Perry, V. H., Holmes, C., Bazan, N. G., Brooks, D. J., Hunot, S., Joseph, B., Deigendesch, N., Garaschuk, O., Boddeke, E., Dinarello, C. A., Breitner, J. C. S., Cole, G. M., Golenbock, D. T., and Kummer, M. P. (2015) Neuroinflammation in Alzheimer's disease. *Lancet Neurol. 14* (4), 388−405.

(3) Wang, Q., Liu, Y., and Zhou, J. (2015) Neuroinflammation in Parkinson's disease and its potential as therapeutic target. *Transl. Neurodegener. 4* (1), 19.

(4) Glass, C. K., Saijo, K., Winner, B., Marchetto, M. C., and Gage, F. H. (2010) Mechanisms underlying inflammation in neurodegeneration. *Cell 140* (6), 918−34.

(5) Cacquevel, M., Lebeurrier, N., Cheenne, S., and Vivien, D. (2004) Cytokines in neuroinflammation and Alzheimer's disease. *Curr. Drug Targets 5* (6), 529−34.

(6) Hensley, K. (2010) Neuroinflammation in Alzheimer's disease: mechanisms, pathologic consequences, and potential for therapeutic manipulation. *J. Alzheimer's Dis. 21* (6), 1−14.

(7) Mcgeer, E. G., and Mcgeer, P. L. (2010) Neuroinflammation in Alzheimer's disease and mild cognitive impairment: a field in its infancy. *J. Alzheimer's Dis. 19* (1), 355−61.

(8) Jucker, M., and Walker, L. C. (2013) Self-propagation of pathogenic protein aggregates in neurodegenerative diseases. *Nature 501* (7465), 45−51.

(9) Gonzalezscarano, F., and Baltuch, G. (1999) Microglia as mediators of inflammatory and degenerative diseases. *Annu. Rev. Neurosci. 22* (1), 219−40.

(10) Akiyama, H., Barger, S., Barnum, S., Bradt, B. M., Bauer, J., Cole, G. M., Cooper, N. R., Eikelenboom, P., Emmerling, M. R., Fiebich, B. L., Finch, C. E., Frautschy, S. A., Griffin, W. S. T., Hampel, H., Hull, M., Landreth, G. E., Lue, L., Mrak, R. E., Mackenzie, I. R. A., Mcgeer, P. L., Obanion, M. K., Pachter, J. S., Pasinetti, G. M., Salaman, C. P., Rogers, J., Rydel, R. E., Shen, Y., Streit, W. J., Strohmeyer, R., Tooyoma, I., Van Muiswinkel, F. L., Veerhuis, R., Walker, D. G., Webster, S. P., Wegrzyniak, B., Wenk, G. L., and Coray, T. W. (2000) Inflammation and Alzheimer's disease. *Neurobiol. Aging 21* (3), 383−421.

(11) Wyss-Coray, T. (2006) Inflammation in Alzheimer disease: driving force, bystander or beneficial response? *Nat. Med. 12* (9), 1005−15.

(12) Ballatore, C., Lee, V. M. Y., and Trojanowski, J. Q. (2007) Tau-mediated neurodegeneration in Alzheimer's disease and related disorders. *Nat. Rev. Neurosci. 8* (9), 663−72.

(13) Morales, I., Guzman-Martinez, L., Cerda-Troncoso, C., Farias, G., and Maccioni, R. B. (2014) Neuroinflammation in the pathogenesis of Alzheimer's disease: A rational framework for the search of novel therapeutic approaches. *Front. Cell. Neurosci. 8*, 112.

(14) Liao, J. C., Deng, J. S., Chiu, C. S., Hou, W. C., Huang, S., Shie, P. H., and Huang, G. J. (2012) Anti-inflammatory activities of cinnamomum cassia constituents in vitro and in vivo. *Evid. Based Complement. Alterna. Med. 2012* (2012), 1−12.

(15) Guzman, J. D. (2014) Natural cinnamic acids, synthetic derivatives and hybrids with antimicrobial activity. *Molecules 19* (12), 19292−349.

(16) Nanjundaiah, S. M., Annaiah, H. N., and Dharmesh, S. M. (2011) Gastroprotective effect of ginger rhizome (Zingiber officinale) extract: Role of gallic acid and cinnamic acid in H(+), K(+)-ATPase/H. pylori inhibition and anti-oxidative mechanism. *Evid. Based Complement. Alternat. Med. 2011* (2011), 1−12.

(17) De, P., Baltas, M., and Bedosbelval, F. (2011) Cinnamic acid derivatives as anticancer agents-a review. *Curr. Med. Chem. 18* (11), 1672−703.

(18) Perluigi, M., Joshi, G., Sultana, R., Calabrese, V., De Marco, C., Coccia, R., Cini, C., and Butterfield, D. A. (2006) In vivo protective effects of ferulic acid ethyl ester against amyloid-beta peptide 1−42-induced oxidative stress. *J. Neurosci. Res. 84* (2), 418−26.

(19) Wang, Y., Wang, Y., Li, J., Hua, L. L., Han, B., Zhang, Y. Z., Yang, X. P., Zeng, Z. L., Bai, H. Y., Yin, H. L., and Lou, J. Y. (2016) Effects of caffeic acid on learning deficits in a model of Alzheimer's disease. *Int. J. Mol. Med. 38* (3), 869−75.

(20) Zhang, X., He, X., Chen, Q., Lu, J. F., Rapposelli, S., and Pi, R. (2018) A review on the hybrids of hydroxycinnamic acid as multi-targetdirected ligands against Alzheimer's disease. *Bioorg. Med. Chem. 26* (3), 543−50.

(21) Chakrabarti, S., Jana, M., Roy, A., and Pahan, K. (2018) Upregulation of suppressor of cytokine signaling 3 in microglia by cinnamic acid. *Curr. Alzheimer Res. 15* (10), 894−904.

(22) Mazur, R. H., Reuter, J. A., Swiatek, K. A., and Schlatter, J. M. (1973) Synthetic sweeteners. 3. Aspartyl dipeptide esters from L-and D-alkylglycines. *J. Med. Chem. 16* (11), 1284−7.

(23) Glowaky, R. C., Hendrick, M. E., Smiles, R. E., and Torres, A. (1991) Development and uses of Alitame: A novel dipeptide amide sweetener. *Sweeteners 450*, 57−67.

(24) Fujihara, S. M., Cleaveland, J. S., Grosmaire, L. S., Berry, K. K., Kennedy, K. A., Blake, J. J., Loy, J., Rankin, B. M., Ledbetter, J. A., and Nadler, S. G. (2000) A D-amino acid peptide inhibitor of NF-κB nuclear localization is efficacious in models of inflammatory disease. *J. Immunol. 165* (2), 1004−112.

(25) Kim, E. Y., Rajasekaran, G., and Shin, S. Y. (2017) LL-37-derived short antimicrobial peptide KR-12-a5 and its d-amino acid substituted analogs with cell selectivity, anti-biofilm activity, synergistic effect with conventional antibiotics, and anti-inflammatory activity. *Eur. J. Med. Chem. 136*, 428−41.

(26) Li, J., Kuang, Y., Gao, Y., Du, X. W., Shi, J. F., and Xu, B. (2013) D-amino acids boost the selectivity and confer supramolecular hydrogels of a nonsteroidal anti-inflammatory drug (NSAID). *J. Am. Chem. Soc. 135* (2), 542−5.

(27) Guo, Z. (2017) The modification of natural products for medical use. *Acta Pharm. Sin. B 7* (2), 119−36.

(28) Dias, K. S., de Paula, C. T., Dos Santos, T., Souza, I. N. O., Boni, M. S., Guimaraes, M. J. R., Da Silva, F. M. R., Castro, N. G., Neves, G., De Carvalho Veloso, C., Coelho, M. M., Melo, I. S. F., Giusti, F. C. V., Giustipaiva, A., Da Silva, M. L., Dardenne, L. E.,

Guedes, I. A., Pruccoli, L., Morroni, F., Tarozzi, A., and Viegas, C. (2017) Design, synthesis and evaluation of novel feruloyl-donepezil hybrids as potential multitarget drugs for the treatment of Alzheimer's disease. *Eur. J. Med. Chem. 130*, 440−57.
(29) Cheng, B., Lin, Y. S., Kuang, M., Fang, S., Gu, Q., Xu, J., and Wang, L. Y. (2015) Synthesis and anti-neuroinflammatory activity of lactone benzoyl hydrazine and 2-nitro-1-phenyl-1H-Indole derivatives as p38α MAPK inhibitors. *Chem. Biol. Drug Des. 86* (5), 1121−30.
(30) Chen, M., Chang, Y., Huang, S., Xiao, L. H., Zhou, W., Zhang, L. Y., Li, C., Zhou, R. P., Tang, J., Lin, L., Du, Z. Y., and Zhang, K. (2018) Aromatic-turmerone attenuates LPS-induced neuroinflammation and consequent memory impairment by targeting TLR4-dependent signaling pathway. *Mol. Nutr. Food Res. 62* (2), 1−9.
(31) Kapogiannis, D., and Mattson, M. P. (2011) Disrupted energy metabolism and neuronal circuit 32 dysfunction in cognitive impairment and Alzheimer's disease. *Lancet Neurol. 10* (2), 187−98.
(32) Block, M. L., Zecca, L., and Hong, J. S. (2007) Microglia-mediated neurotoxicity: uncovering the molecular mechanisms. *Nat. Rev. Neurosci. 8* (1), 57−69.
(33) Lu, Y. C., Yeh, W. C., and Ohashi, P. S. (2008) LPS/TLR4 signal transduction pathway. *Cytokine 42* (2), 145−51.
(34) Raz, N., Ghisletta, P., Rodrigue, K. M., Kennedy, K. M., and Lindenberger, U. (2010) Trajectories of brain aging in middle-aged and older adults: regional and individual differences. *Neuroimage 51* (2), 501−11.
(35) Sparkman, N. L., Martin, L. A., Calvert, W. S., and Boehm, G. W. (2005) Effects of intraperitoneal lipopolysaccharide on Morris maze performance in year-old and 2-month-old female C57BL/6J mice. *Behav. Brain Res. 159* (1), 145−51.
(36) Semmler, A., Hermann, S., Mormann, F., Weberpals, M., Paxian, S. A., Okulla, T., Schafers, M., Kummer, M. P., Klockgether, T., and Heneka, M. T. (2008) Sepsis causes neuroinflammation and concomitant decrease of cerebral metabolism. *J. Neuroinflammation 5* (1), 38.
(37) Lee, J. W., Lee, Y. K., Yuk, D. Y., Choi, D. Y., Ban, S. B., Oh, K. W., and Hong, J. T. (2008) Neuro-inflammation induced by lipopolysaccharide causes cognitive impairment through enhancement of beta-amyloid generation. *J. Neuroinflammation 5* (1), 37.
(38) Reitz, C., Brayne, C., and Mayeux, R. (2011) Epidemiology of Alzheimer disease. *Nat. Rev. Neurol. 7* (3), 137−52.
(39) Eichenbaum, H. (2000) A cortical-hippocampal system for declarative memory. *Nat. Rev. Neurosci. 1* (1), 41−50.
(40) Eichenbaum, H. (2004) Hippocampus: cognitive processes and neural representations that underlie declarative memory. *Neuron 44* (1), 109−20.
(41) Palop, J. J., and Mucke, L. (2010) Amyloid-beta-induced neuronal dysfunction in Alzheimer's disease: From synapses toward neural networks. *Nat. Neurosci. 13* (7), 812−8.
(42) Wang, Q., Liu, Y., and Zhou, J. (2015) Neuroinflammation in Parkinson's disease and its potential as therapeutic target. *Transl. Neurodegener. 4* (1), 19.
(43) Qin, L., Wu, X., Block, M. L., Liu, Y., Breese, G. R., Hong, J. S., Knapp, D. J., and Crews, F. T. (2007) Systemic LPS causes chronic neuroinflammation and progressive neurodegeneration. *Glia 55* (5), 453−62.
(44) Davidowitz, E. J., Moe, J. G., Reitz, A. B., Bian, H., Gluchowski, C., Hendrix, J., Yehaskel, A. S., Mcdonnell, M. E., and Loughran, M. H. (2019) Novel quinazolinones that inhibit the formation of tau oligomers and their method of use. U.S. Patent Application No. 16/471 363.
(45) Fang, Y., Zhou, H., Gu, Q., and Xu, J. (2019) Synthesis and evaluation of tetrahydroisoquinoline-benzimidazole hybrids as multifunctional agents for the treatment of Alzheimer's disease. *Eur. J. Med. Chem. 167* (2019), 133−45.
(46) Liu, W. F., Huang, S., Li, Y. L., Zheng, X., and Zhang, K. (2019) Suppressive effect of glycyrrhizic acid against lipopolysaccharide-induced neuroinflammation and cognitive impairment in C57 mice via toll-like receptor 4 signaling pathway. *Food Nutr. Res. 63* (63), 1516−28.

https://dx.doi.org/10.1021/acschemneuro.0c00578
ACS Chem. Neurosci. 2021, 12, 419−429